Dynamics of Self-Generated Magnetic Fields in Stagnation Phase and their Effects on Hot Spark Formation

Akiro HATA, Kunioki MIMA, Astushi SUNAHARA[1)],
Hideo NAGATOMO and Akio NISHIGUCHI[2)]

Institute of Laser Engineering, Osaka University, Suita 565-0871, Japan
[1)]*Institute of Laser Technology, Suita 565-0871, Japan*
[2)]*Osaka Institute of Technology, Osaka 535-8585, Japan*

(Received 29 September 2005 / Accepted 3 February 2006)

The generalized temporal evolution equation of a magnetic field is derived for high density laser-fusion plasmas. Magnetic field generation and convection are simulated by using the 2D hydrodynamic code together with the magnetic field equation. It is found that magnetic fields are generated and compressed in association with the Rayleigh-Taylor instability of an imploding shell. In particular, the magnetic field convection by the Nernst effect is found to play an important role in the amplification of magnetic fields. The maximum magnetic field reaches 30 MG at maximum compression. This magnetic field may reduce the electron heat conduction around the hot spark. Therefore, it is concluded that the ignition condition for non-uniform implosion is influenced by self-generated magnetic fields.

Keywords: laser fusion, magnetic field, Rayleigh-Taylor instability, Nernst effect, convection, heat transport

DOI: 10.1585/pfr.1.020

1. Introduction

It is widely known that megagauss magnetic fields are generated in laser plasmas. In the 1970s, Stamper *et al.* measured a kilogauss magnetic field in a laser-produced plasma [1]. After that, various measurements and simulations have revealed that magnetic fields in high intensity laser-produced plasmas reach the order of 1–100 megagauss [2, 3]. A mechanism that plays a role in self-generated magnetic fields can be explained by the non-parallel density and temperature gradients [4].

In fast ignition, megagauss-order magnetic fields exert significant effects on the electron heat flux [5]. In laser plasmas, a magnetic field is not only generated by non-uniform laser irradiation but also by various instabilities such as collisionless and collisional Weibel instabilities [6, 7], thermal instability [8], and Rayleigh-Taylor instability [9]. When a laser irradiates a solid target, nonparallel temperature and density gradients appear due to the Rayleigh-Taylor (RT) instability [10]. The RT instability in the acceleration and the deceleration phases can be the major source of the magnetic field in imploded plasmas. The magnetic fields in the acceleration phase of the implosion are convected into the ablation front by the Nernst effect [11]. These magnetic fields then penetrate further inward. The magnetic fields are amplified in the deceleration phase as well, where all the magnetic fields are compressed rapidly. Therefore, the magnetic fields become strong enough to influence the implosion process.

In this paper, we discuss magnetic field generation and its effects on heat transport due to RT instability in the deceleration phase. In Sec. 2, the basic equations for the magnetic field's temporal evolution are derived. Magnetic field generation and amplification are simulated in Sec. 3. Section 4 is devoted to an analysis of the simulation results. Finally, Sec. 5 provides a summary and a conclusion.

2. Simulation Model

The temporal evolution of magnetic fields is described by the following Maxwell equation (1) and the equation of electron motion shown in Eq. (2).

$$\frac{\partial \boldsymbol{B}}{\partial t} = -c\nabla \times \boldsymbol{E}, \tag{1}$$

where $\boldsymbol{B}$, c, and $\boldsymbol{E}$ are the magnetic field, the speed of light, and the electric field, respectively. The equation of electron motion is given by

$$m_e n_e \frac{\mathrm{d}\boldsymbol{V}_e}{\mathrm{d}t} = -en_e\left(\boldsymbol{E} + \frac{1}{c}\boldsymbol{V}_e \times \boldsymbol{B}\right) - \nabla p_e + \boldsymbol{R}_{ei} \simeq 0, \tag{2}$$

where n_e, m_e, $\boldsymbol{V}_e$, and p_e are the number density, mass, velocity, and isotropic pressure of electrons, respectively. $\boldsymbol{R}_{ei}$ is the force due to ion collisions. Here, we assume that the electron inertia is negligible in Eq. (2) and the charge neutrality $n_e = Zn_i$. We define electric current density $\boldsymbol{J}$ as

$$\boldsymbol{u} = \boldsymbol{V}_e - \boldsymbol{V}_i = -\boldsymbol{J}/n_e e = -(c/4\pi n_e e)\nabla \times \boldsymbol{B}. \tag{3}$$

author's e-mail: ahata@ile.osaka-u.ac.jp

The electric field $\boldsymbol{E}$ and $\boldsymbol{V}_e$ are eliminated from Eqs. (1), (2), and (3) to obtain

$$\frac{\partial \boldsymbol{B}}{\partial t} = \nabla \times (\boldsymbol{V}_i \times \boldsymbol{B}) + \frac{c}{e}\Big[\nabla \times \Big(\frac{\nabla p_e}{n_e}\Big) - \nabla \times \Big\{\frac{(\nabla \times \boldsymbol{B}) \times \boldsymbol{B}}{4\pi n_e}\Big\} - \nabla \times \Big(\frac{\boldsymbol{R}_T + \boldsymbol{R}_u}{n_e}\Big)\Big], \quad (4)$$

where the collision term $\boldsymbol{R}_{ei}$ is separated into the thermal force $\boldsymbol{R}_T$ and the friction force $\boldsymbol{R}_u$. $\boldsymbol{R}_T$ and $\boldsymbol{R}_u$ in Eq. (4) are defined as follows:

$$\boldsymbol{R}_T = -\beta_{\shortparallel}^{uT}\nabla_{\shortparallel}T_e - \beta_{\perp}^{uT}\nabla_{\perp}T_e - \beta_{\wedge}^{uT}\boldsymbol{h} \times \nabla T_e, \quad (5)$$

$$\boldsymbol{R}_u = -\alpha_{\shortparallel}\boldsymbol{u}_{\shortparallel} - \alpha_{\perp}\boldsymbol{u}_{\perp} + \alpha_{\wedge}\boldsymbol{h} \times \boldsymbol{u}, \quad (6)$$

where $\boldsymbol{h}$ is a unit vector in the direction of the magnetic field. The vectors $\boldsymbol{u}_{\shortparallel}$ and $\boldsymbol{u}_{\perp}$ represent $\boldsymbol{h}(\boldsymbol{u}\cdot\boldsymbol{h})$ and $\boldsymbol{h} \times (\boldsymbol{u} \times \boldsymbol{h})$, respectively. T_e is electron temperature, and $\nabla_{\shortparallel}T_e$ represents $\boldsymbol{h}(\boldsymbol{h}\cdot\nabla T_e)$. Also $\nabla_{\perp}T_e$ represents $\boldsymbol{h}\times(\nabla T_e \times \boldsymbol{h})$. α and β are given by

$$\begin{aligned}
&\beta_{\shortparallel}^{uT} = n_e\beta_0, \qquad \beta_{\perp}^{uT} = n_e(\beta_1'\chi^2 + \beta_0')/\Delta,\\
&\beta_{\wedge}^{uT} = n_e\chi(\beta_1''\chi^2 + \beta_0'')/\Delta,\\
&\alpha_{\shortparallel} = \frac{m_e n_e \alpha_0}{\tau_e}, \qquad \alpha_{\perp} = \frac{m_e n_e}{\tau_e}\Big(1 - \frac{\alpha_1'\chi^2 + \alpha_0'}{\Delta}\Big),\\
&\alpha_{\wedge} = \frac{m_e n_e}{\tau_e}\frac{\chi(\alpha_1''\chi^2 + \alpha_0'')}{\Delta},\\
&\chi = \omega_e\tau_e, \qquad \Delta = \chi^4 + \delta_1\chi^2 + \delta_0.
\end{aligned} \quad (7)$$

Here χ is the Hall parameter, $\omega_e = eB/mc$ is the electron cyclotron frequency, τ_e is electron-ion collision mean free time, and $\beta_0, \beta_1', \beta_0', \beta_1'', \beta_0'', \alpha_0, \alpha_1', \alpha_0', \alpha_1'', \alpha_0'', \delta_0$, and δ_1 are thermal transport coefficients, respectively. These coefficients are listed in detail in Ref. [12]. The first term on the right-hand side of Eq. (4) represents the convection and the stretching of the magnetic field by hydrodynamic motion. The second term, $(c/e)\nabla \times (\nabla p_e/n_e)$, is the source of the magnetic field, called Rihi Ludac effects. If we treat electron pressure as ideal gas, we obtain the well-known result $(c/(en_e))\nabla T_e \times \nabla n_e$. This means that eddy currents are generated when nonparallel gradients of electron density and temperature exist. The third term on the right-hand side of Eq. (4) shows the ion Hall effect. The Hall effect is important when the magnetic spatial scale is comparable to ion skin depth. The last term on the right-hand side of Eq. (4) contains the diffusion of the magnetic field and the Nernst effect, which plays an important role in the motion of the magnetic field. The Nernst effect is due to the generation of current perpendicular to the temperature gradient and the magnetic field.

We next concentrate our analysis on the thermal force $\boldsymbol{R}_T$ and the friction force $\boldsymbol{R}_u$. Inserting Eqs. (5) and (6) into Eq. (4) together with taking into account the relation of the velocity $\boldsymbol{u}$ in Eq. (3) to the magnetic field, the last term on the right-hand side of the Eq. (4) is written as

$$\begin{aligned}
\nabla \times \Big(\frac{\boldsymbol{R}_T + \boldsymbol{R}_u}{n_e}\Big) &= -\nabla \times (\beta' \nabla T_e)\\
&- \frac{e}{c}\nabla \times \Big(\boldsymbol{B} \times \beta'' \frac{\tau_e}{m_e}\nabla T_e\Big) + \nabla \times \Big(\frac{m_e c}{4\pi e}\frac{\alpha_0}{n_e\tau_e}\boldsymbol{h}\{(\nabla \times \boldsymbol{B})\cdot\boldsymbol{h}\}\Big)\\
&+ \nabla \times \Big(\frac{m_e c}{4\pi e}\frac{1-\alpha'}{n_e\tau_e}\boldsymbol{h} \times \{(\nabla \times \boldsymbol{B}) \times \boldsymbol{h}\}\Big)\\
&+ \nabla \times \Big\{\frac{\alpha''}{4\pi n_e}(\nabla \times \boldsymbol{B}) \times \boldsymbol{B}\Big\}.
\end{aligned} \quad (8)$$

Here, coefficients β', β'', α', and α'' depending on $\omega_e\tau_e$ are given by

$$\begin{aligned}
\beta' &= (\beta_1'\chi^2 + \beta_0')/\Delta, \qquad \beta'' = (\beta_1''\chi^2 + \beta_0'')/\Delta,\\
\alpha' &= (\alpha_1'\chi^2 + \alpha_0')/\Delta, \qquad \alpha'' = (\alpha_1''\chi^2 + \alpha_0'')/\Delta.
\end{aligned} \quad (9)$$

First of all, combining the first term on the right-hand side of Eq. (8) with the $\nabla T_e \times \nabla n_e$ term, the source of the magnetic field is rewritten as

$$\frac{c}{e}\frac{1}{n_e}\nabla T_e \times \nabla n_e + \frac{c}{e}\nabla \times (\beta' \nabla T_e) = \frac{c}{e}\nabla T_e \times \nabla(\log n_e - \beta'). \quad (10)$$

The second term $\nabla \times (\beta' \nabla T_e)$ on the left-hand side of Eq. (10) denotes the thermal force associated with the electron-ion friction force in the presence of the thermal gradient. Note that $\nabla \times (\beta' \nabla T_e)$ is 0 when $\boldsymbol{B} = 0$. In addition, the contribution of $\nabla \times (\beta' \nabla T_e)$ to magnetic field generation is usually smaller than the $\nabla T_e \times \nabla n_e$ term in a high density plasma.

Nishiguchi *et al.* [11] have studied the convection processes of a magnetic field in a laser-produced plasmas in terms of the Nernst effect. This term is written as follows:

$$\nabla \cdot \Big(B\beta'' \frac{\tau_e}{m_e}\nabla T_e\Big) = -\nabla \cdot (B\boldsymbol{V}_T), \quad \boldsymbol{V}_T = -\beta'' \frac{\tau_e}{m_e}\nabla T_e. \quad (11)$$

According to their work, the magnetic field is convected toward the lower temperature region with velocity $\boldsymbol{V}_T$ which is comparable to the fluid velocity $\boldsymbol{V}_i$ in a laser-driven ablation. The velocity $\boldsymbol{V}_T$ is the heat flow velocity and $\nabla \cdot \boldsymbol{V}_T$ is negative on the ablation front. As a result, the magnetic field is amplified at the ablation front. The third term and the fourth term represent diffusion parallel to the magnetic field and that perpendicular to the magnetic field, respectively. Both terms are derived from the friction force $\boldsymbol{R}_u$.

The last term also originates from the friction force. Ultimately the temporal evolution of the magnetic field is subjected to

$$\begin{aligned}
\frac{\partial \boldsymbol{B}}{\partial t} &= \nabla \times \{(\boldsymbol{V}_i + \boldsymbol{V}_T) \times \boldsymbol{B}\} + \frac{c}{e}\Big[\nabla T_e \times \nabla(\log n_e - \beta')\\
&- \nabla \times \Big\{\frac{1+\alpha''}{4\pi n_e}(\nabla \times \boldsymbol{B}) \times \boldsymbol{B}\Big\} - \nabla \times \Big(\frac{m_e c}{4\pi e}\frac{\alpha_0}{n_e\tau_e}\boldsymbol{h}\{(\nabla \times \boldsymbol{B})\cdot\boldsymbol{h}\}\\
&- \nabla \times \Big(\frac{m_e c}{4\pi e}\frac{1-\alpha'}{n_e\tau_e}\boldsymbol{h} \times \{(\nabla \times \boldsymbol{B}) \times \boldsymbol{h}\}\Big)\Big].
\end{aligned} \quad (12)$$

In summary, it is found that the temporal evolution of the magnetic field is composed of the source, the Nernst effect, diffusion, and the pressure of magnetic field. It is important to notice here that the thermo-electric current $\nabla T_e \times \nabla n_e$ is the only source of the magnetic field.

3. Simulation of Magnetic Field Generation in the Stagnation Phase

In order to simulate the temporal evolution of the magnetic field, we use space-time dependent plasma profiles which are obtained by hydrodynamic simulation. The imploded fuel pellet is a CH capsule which contains DT fuel. The thickness of the CH capsule shell, solid DT, and gas DT are 2 μm, 100 μm, and 795 μm, respectively.

Figure 1 shows the pulse shape of a 0.35 μm wavelength implosion laser. The laser pulse energy is 50 kJ with a corresponding intensity of 1.4×10^{14} W/cm^2. The laser pulse duration is 3.72 ns.

We used the ILESTA-1D code [13] until stagnation phase $t = 3.9$ ns, then 2D simulation was carried out for the plasma profile obtained by 1D calculation. The streamline of the implosion is shown in Fig. 2. At the beginning of the stagnation phase ($t = 3.9$ ns) we switched to the 2-D simulation code where we used the ideal fluid equations [14]. The fluid equations are given by

$$\frac{\partial \boldsymbol{U}}{\partial t} + \frac{\partial \boldsymbol{F}^x}{\partial x} + \frac{\partial \boldsymbol{F}^y}{\partial y} = 0,$$

$$\boldsymbol{U} = \begin{pmatrix} \rho \\ \rho u \\ \rho v \\ \rho E \end{pmatrix}, \boldsymbol{F}^x = \begin{pmatrix} \rho u \\ p + \rho u^2 \\ \rho uv \\ \rho uE + up \end{pmatrix}, \boldsymbol{F}^y = \begin{pmatrix} \rho v \\ \rho uv \\ p + \rho v^2 \\ \rho vE + vp \end{pmatrix},$$

$$E = \frac{p}{(\gamma - 1) \cdot \rho} + \frac{1}{2}(u^2 + v^2), \tag{13}$$

where ρ and E are mass density and the total energy, respectively. u and v are the velocities of the direction of x and y, respectively. The specific heat capacity ratio γ is assumed to be 5/3. We set 10% velocity perturbation at 3.9 ns and calculated the magnetic field from 3.9 ns to 4.4 ns where the Rayleigh-Taylor instability of mode 6 is included in the deceleration phase. The temporal evolutions of magnetic fields depend on velocity $v \approx 10^7$ cm/s and a spatial scale length which is determined by the temperature and density gradients. When we solve the magnetic field equation (12), the time step should be shorter than L/v which is longer than 10 ps when $L \gtrsim 1$ μm. In this case, it is justified that the time step is 10 ps. In our model, we investigated the generation of a magnetic field in axisymmetric cylindrical geometry (r, z) so that we have only a B_ϕ component. The total size of the simulation is 384 μm×768 μm with a mesh spacing of $\Delta r = \Delta z = 1.5$ μm in the r and z directions, respectively. B_ϕ is defined at a cell center, and ion velocity is defined on a cell corner. The boundary condition of B_ϕ is a free boundary, along the z axis.

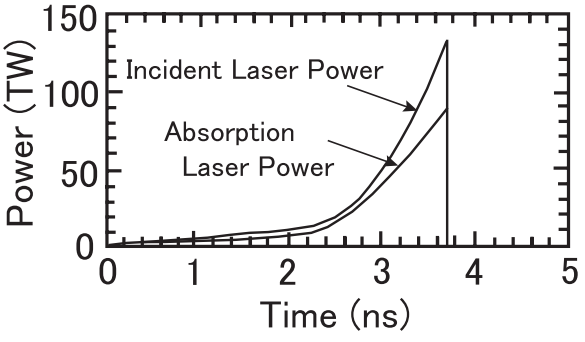

Fig. 1 The pulse shape of 3ω laser with energy of 50 kJ.

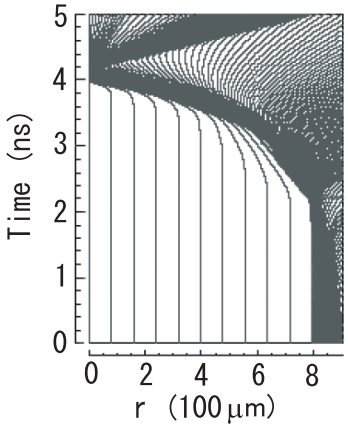

Fig. 2 The R-T diagram of the implosion obtained by the ILESTA-1D code. This 1D code was used until 3.9 ns as an initial condition for the calculation of a magnetic field.

4. Analysis of Simulation Results at Different Times

Figure 3 shows electron density and electron temperature profiles in the deceleration phase. The simulation of the magnetic field started when the shell was compressed toward the center at $t = 3.9$ ns. The compression of the fuel continued until 4.16 ns, where the peak electron density and temperature reach 3.3×10^{25} cm^{-3} and 8000 eV, respectively, near the center. After maximum compression, the target expands outward. Ignition and burn are not included in this simulation.

The distributions of the self-generated magnetic field are shown in Fig. 4. The positive value of B_ϕ indicates a right-handed circular direction. Magnetic fields are created near the steep gradient of electron temperature, which rise up to 30 MG at maximum compression. In the early stage of the deceleration phase, magnetic fields generated by the source term are generated around both sides of spikes of the Rayleigh-Taylor mode shown in Fig. 4 (b). The magnitude of the magnetic field reaches its maximum at maximum compression, and the magnetic fields are compressed rapidly toward the center by the stagnation motion.

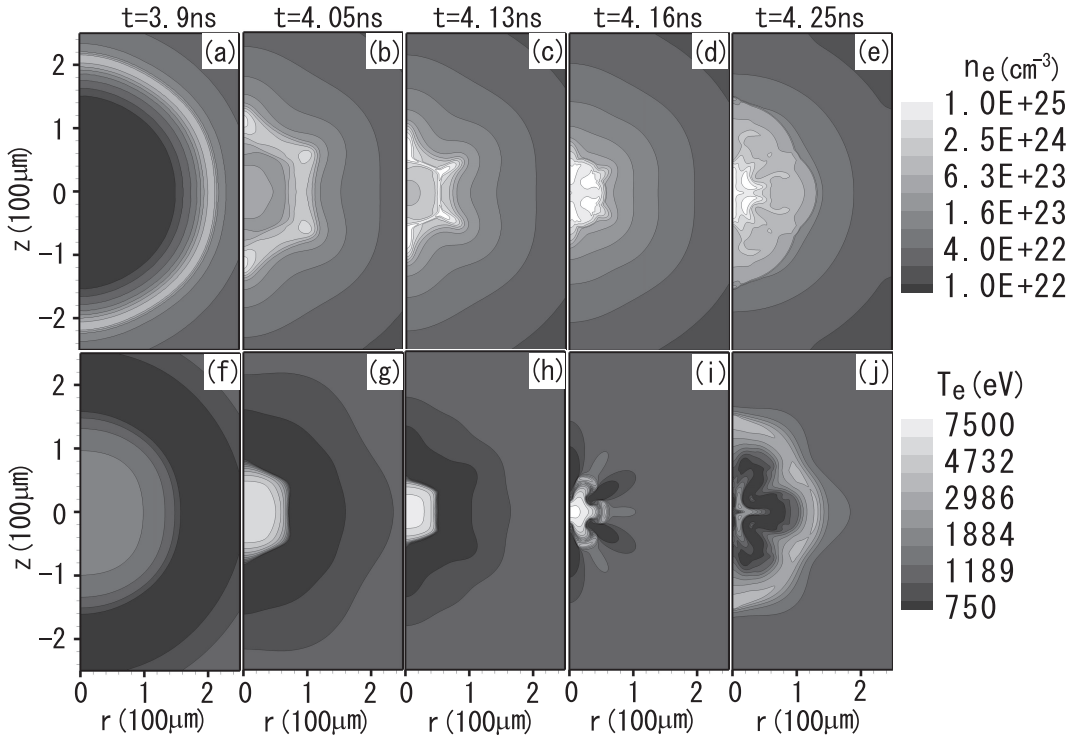

Fig. 3 The contour profiles of (a)-(e): the electron density n_e [cm^{-3}], and (f)-(j): the electron temperature T_e [eV] at t = 3.9, 4.05, 4.13, 4.16, and 4.25 ns, respectively.

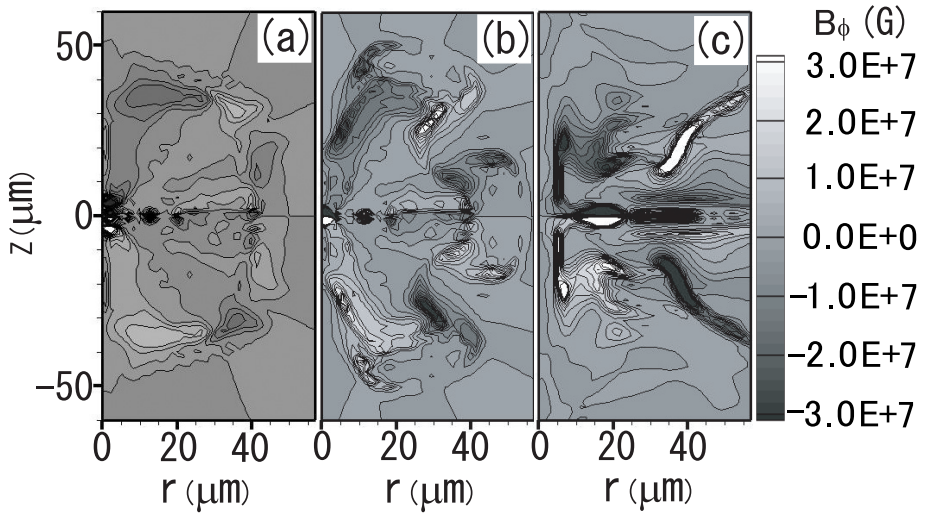

Fig. 4 The profiles of B_ϕ(G) at (a) t = 4.13 ns, (b) t = 4.16 ns, and (c) t = 4.25 ns, respectively.

Figure 5 represents the relations among ion velocity $\boldsymbol{V}_i$, the Nernst velocity $\boldsymbol{V}_T$, and the total velocity $\boldsymbol{V}_i + \boldsymbol{V}_T$ at 4.16 ns. The ion fluid flows toward the center until the maximum compression and the velocity $|\boldsymbol{V}_i|$ extends to 6.0×10^7 cm/s. The Nernst velocity is defined as a function of the magnetic field and the heat flow caused by the gradients of electron temperature. The heat flow is opposite ion velocity on the inner surface of the imploding shell so that $\boldsymbol{V}_i$ and $\boldsymbol{V}_T$ cancel each other on the shell's inner surface. On the other hand, on the outer surface of the shell, $\boldsymbol{V}_i$ and $\boldsymbol{V}_T$ are the same sign and $\boldsymbol{V}_i + \boldsymbol{V}_T$ is large on the outside of the shell as shown in Fig. 5 (c). Therefore, the magnetic fields are compressed on the inner surface of the imploding shell as shown in Fig. 4 (b). Along the z axis, cylindrical spikes collide around the center. As a result, very strong magnetic fields are generated on the z axis near the center of the core plasma. As the result, the combination of imploding plasma flow and the Nernst effect amplify the magnetic field effectively during stagnation.

The distribution of the Hall parameter defined by $\omega_e\tau_e$

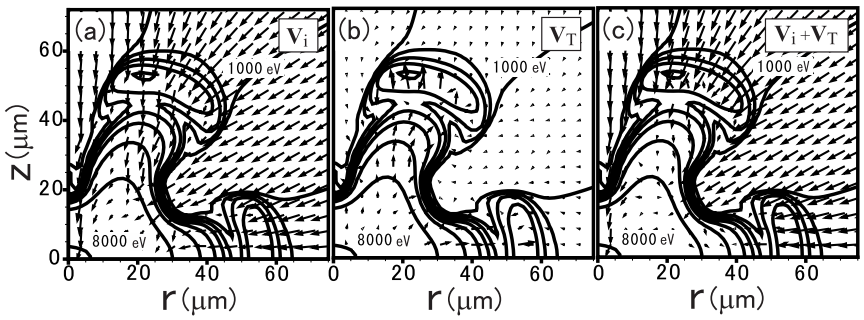

Fig. 5 The comparison of the ion velocity(vector) with the Nernst velocity(vector), and the temperature profile(contour lines) at t = 4.16 ns. (a) ion velocity; $\boldsymbol{V}_i$ [cm/s], (b)the Nernst velocity; $\boldsymbol{V}_T$ [cm/s], and (c) $\boldsymbol{V}_i + \boldsymbol{V}_T$ [cm/s]. The shortest arrow indicates 1.0×10^7 cm/s.

is shown in Fig. 6. The heat conduction is reduced by a factor of $1/\{1 + (\omega_e\tau_e)^2\}$. This factor could be as small as $1/2$ in the strong magnetic fields. Therefore, the self-generated magnetic field could play an important role in hot spark ignition.

5. Summary and Conclusion

Temporal evolution equations of self-generated magnetic field are derived by including convection as well as the Nernst effect for imploding plasmas. We simulated magnetic filed generation in association with the Rayleigh-Taylor instability. The maximum magnetic field reaches 30 MG around the hot spark at maximum compression. The amplitudes of the magnetic field are estimated by the balance between amplification rate and diffusion. By this estimation, the magnetic field intensity is roughly obtained as $B \approx T_e\omega_{pe}^2/(ec\nu_{ei}) \propto T_e^{2.5}$. Namely, $B \approx 30$ MG at maximum compression. Here, ω_{pe} and ν_{ei} are electron plasma frequency and e-i collision frequency, respectively. If temperature increases as high as ignition temperature $T_e = 10$ keV from $T_e = 5$ keV which is the maximum temperature of this simulation, the magnetic field increases 5-fold because the intensity of the magnetic field is proportional to $T_e^{2.5}$. Therefore, the peak magnetic field reaches 150 MG.

Since electron heat conduction is strongly affected by this magnetic field, the electron temperature profile is modified and hydrodynamic motion may be strongly affected in burning plasmas.

The electron's Lamor radius for a 30 MG magnetic field is estimated as $r_L \simeq 50\,\mu$m, thus there exists the possibility that particles may be trapped by the magnetic field. Therefore, the influence of the self-generated magnetic field on ignition should be critically investigated. In three-dimensional simulations, stretching and dynamo effects will appear to affect the magnetic field structure on an ablation surface. The three-dimensional effects will be important in this case and should be investigated in future studies.

Finally, we note that the strong magnetic field in the imploded plasma plays an extremely important role in relativistic electron heating in fast ignition.

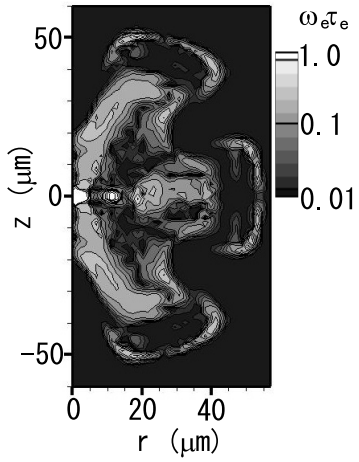

Fig. 6 The distribution of the Hall parameter $\omega_e\tau_e$.

Therefore, the effects of a self-generated magnetic field on relativistic electron transport should also be investigated in the future.

[1] J.A. Stamper, K. Papadopoulos, R.N. Sudan, S.O. Dean, E.A. McLean and J.M. Dawson, Phys. Rev. Lett. **26**, 1012 (1971).
[2] Y. Sakagami, H. Kawakami, S. Nagao and C. Yamanaka, Phys. Rev. Lett. **42**, 839 (1979).
[3] M. Tatarakis *et al.*, Phys. Plasmas **9**, 2244 (2002).
[4] C.E. Max, W.M. Manheimer and J.J. Thomson, Phys. Fluids **21**, 128 (1978).
[5] P. Nicolai, M.Vandenboomgaerde, B. Canaud and F. Chaigneau, Phys. Plasmas **7**, 4250 (2000).
[6] T. Okada, T. Yabe and K. Niu, J. Phys. Soc. Jpn. **43**, 1042 (1977).
[7] T. Mochizuki, T. Yabe, K. Mima, K. Yoshikawa, H. Azechi, A. Kikuchi and C. Yamanaka, Jpn. J. Appl. Phys. **19**, L645 (1980).
[8] M.G. Haines, Phys. Rev. Lett. **47**, 917 (1981).
[9] F. Hattori, H. Takabe and K. Mima, Phys. Fluids **29**, 1719 (1986).

[10] K. Mima, T. Tajima and J.N. Leboeuf, Phys. Rev. Lett. **41**, 1715 (1978).
[11] A. Nishiguchi, T. Yabe and M. Haines, Phys. Fluids **28**, 3683 (1985).
[12] S.I. Braginskii, *Reviews of Plasma Physics* **1** (Consultants Bereau, New York, 1965).
[13] H. Takabe *et al.*, Phys. Fluids **31**, 2884 (1988).
[14] A. Sunahara, H. Takeuchi, H. Takabe and K. Mima, Jpn. J. Appl. Phys. **35**, 6265 (1996).